Ferro- and ferrielectricity and negative piezoelectricity in thioamide-based supramolecular organic discotics

Indre Urbanaviciute[1], Miguel Garcia-Iglesias[2,3], Andrey Gorbunov[4], E. W. Meijer[2,5], Martijn Kemerink*[1,6]

[1] Complex Materials and Devices, Department of Physics, Chemistry and Biology (IFM), Linköping University, 58183 Linköping, Sweden.

[2] Institute for Complex Molecular Systems, Eindhoven University of Technology, Eindhoven P.O. Box 513, 5600 MB Eindhoven, the Netherlands;

[3] QUIPRE Department, Universidad de Cantabria, Avd. de Los Castros, 46, 39005 Santander, Spain.;

[4] Department of Applied Physics, Eindhoven University of Technology, PO Box 513, 5600 MB, Eindhoven, The Netherlands;

[5] Laboratory of Macromolecular and Organic Chemistry, Eindhoven University of Technology, Eindhoven P.O. Box 513, 5600 MB Eindhoven, the Netherlands;

[6] Institute for Molecular Systems Engineering and Advanced Materials, Heidelberg University, Im Neuenheimer Feld 225, 69120 Heidelberg, Germany.

* Corresponding author

E-mail: martijn.kemerink@cam.uni-heidelberg.de

Abstract

Amide-based discotic supramolecular organic materials are of interest for fundamental understanding of cooperative self-assembly and collective dipole switching mechanisms as well as for practically relevant ferroelectric and piezoelectric properties. Here, we show how replacing amides (dipole moment of ~3.5 D) with thioamides (~5.1 D) as dipolar moieties in the archetypal C3-symmetric discotic molecule BTA leads to ferroelectric materials with a higher remnant polarization and lower coercive field. The thioamide-based materials also demonstrate a rare negative piezoelectricity and a previously predicted, yet never

experimentally observed, polarization reversal via asymmetric intermediate states, that is, ferrielectric switching.

Introduction

Ferroelectric columnar discotics feature the essential elements for ferroelectric switching – a stabilizing planar π-stacking conjugated core, strongly polar and free-to-rotate hydrogen-bonding groups equipped with solubilizing aliphatic sidechains that also act as intercolumnar spacers[1]. Their core-shell molecular architecture promotes highly cooperative multi-stage hierarchical ordering, starting with axial 1D self-assemblies of a tail-governed helical preference that pack in tight, typically hexagonal lattices in the solid-state[2]. An important advantage of discotics is their proven sensitivity to changes in molecular structure that opens various possibilities for tailoring their properties [3–6]. By tail or core substitution, the molecular packing can be tuned both geometrically, by increasing the dipole density[3], and energetically, leading to a more supramolecular polymer-like rather than liquid-crystalline behavior, which results in improved piezoelectric properties[4] and substantial polarization stabilization[5,7]. While there are still means for improvement of polarization stability, for example through elimination of chiral defects by employing enantiopure systems[8], the possibilities to increase the dipole density by tail-engineering are limited. Therefore, alternative approaches must be found. The calculated dipole moment per amide in a self-assembled **BTA** (benzene-1,3,5-trisamide) stack is 3.5–4 D[9]. One would search for a replacement to amides that would retain all mentioned advantages yet have a higher dipole moment. A good candidate is the thioamide moiety with sulphur replacing oxygen – a basis for **thioBTAs** (benzene-1,3,5-tri**thio**amides). The latter carries an estimated dipole moment of ~5.1 D (~25% larger than amide) and enables collective hydrogen bonding[10,11].

The supramolecular assembly of discotic (thio)amides has been studies for decades, and these structurally simple materials are an important model system to understand the fundamentals of one-dimensional self-assembly driven by van der Waals interactions in solution and in the solid state. Extensive experimental and computational work has been carried out to comprehend the mechanism behind and outcomes of the strongly cooperative process of self-assembly in these systems[2,9–17]. One finding that is also crucial for the present work is that, compared to racemic systems, homochiral or enantiomerically pure systems generally show a stronger self-organization and concomitantly larger structural order in the solid state, leading to, amongst others, longer polarization retention times and larger coercive fields[8]. Supramolecular stacks of

(thio)BTA have a macrodipole moment that originates from the head-to-tail arrangement of the (thio)amide microdipoles. Here and in the following, the brackets in (thio)BTAs indicate that both thioBTA and normal amideBTA are meant, the same holds for (thio)amides.

It was predicted by atomistic molecular dynamics simulations[9,18] that two configurations of **BTA** supramolecular stacks are possible – a 'symmetric' 3:0 conformer and an 'asymmetric' 2:1 conformer, the numbers denoting the number of hydrogen-bonded 'sub-helixes' in the 1D triple-helical supramolecular assembly that point in the up and down directions, respectively. At the molecular level it can also be understood as the number of H-bond donors and acceptors in a molecule. The 2:1 conformers (*i.e.* ↑↑↓) were shown to have higher stabilization energies than the 3:0 (*i.e.* ↑↑↑) analogues and should therefore be the dominating kind. Initial simulations were carried out for diluted solution conditions, mimicking a realistic solvent environment[9,19,20], and were later followed by studies of liquid crystalline states[8,18].

Apart from the interactions between the sub-helixes inside a single column, also the interactions between full columns can lead to (partially) antiparallel arrangement of macro-dipoles[8,18]. Zehe et al. argued, on basis of a 2D Ising model that accounts for nearest and next-nearest interactions between full columns, that steric effects are responsible for the non-antiparallel, i.e. parallel, organization of columnar dipoles on a hexagonal lattice [21]. In later work, Cornelissen et al. argued,[33] on basis of a kinetic 3D electrostatic model, that the ground state of the hexagonally organized BTA assemblies is a geometrically frustrated anti-ferroelectric one, and that practical systems behave as 'apparent' ferroelectrics due to their slow kinetics[8,18]. For the present discussion, it is important that the geometric frustration discussed in both works does not lead to a specific (meta-)stable macroscopic polarization state between full polarization and full depolarization. Specifically, a 2:1 state is not expected, as it is not compatible with a hexagonal lattice.

In terms of dipolar switching, a 2:1 ground state of the system is expected to manifest itself as ferrielectric switching (analogous to ferrimagnetism), which is generally characterized by different sub-lattices switching at different characteristic (coercive) fields[22,23]; specifically, coming from a high reverse field in which the system is in a ↓↓↓-state, the **(thio)BTA** system would switch to its ↓↓↑ ground state at a finite but negative electric field. At positive fields, the system would first switch to the ↓↑↑-state before switching to the ↑↑↑-state at high positive field. This would give rise to a characteristic three-step hysteresis curve, as opposed to the one-step curve for ferroelectric systems. Previous numerical simulations suggested that the intermediate states ↓↑↑ and ↓↓↑ may be absent in the **(thio)BTA** system due to required non-

chiral dipole switching mode being energetically unfavorable.[8] Similarly, a fully polarized stack would relax to this 2:1 ground state during thermal depolarization. Nevertheless, so far there has not been any experimental proof of the existence of these asymmetric antiparallel 2:1 conformers in amide-based discotics. In fact, except for bent-core smectic liquid crystals[24–28], ferrielectricity is rarely found in organic systems.

Here, we characterize **thioBTA**-based homologues with (linear) achiral and (branched) chiral tails in terms of their ferroelectric and piezoelectric properties. We find that the enantiopure chiral system shows pronounced ferrielectric behavior when it is brought into its liquid-crystalline state, whereas the achiral system is ferroelectric at all temperatures. We attribute the difference to improved self-assembly of chiral systems that provides the long-range order that is required for the stabilization of the 2:1 state. Furthermore, chiral-tailed **thioBTA** demonstrates a rare negative piezoelectric effect both in the ferroelectric and ferrielectric state under large- and small-signal conditions.

Results

Synthesis

We investigate two **thioBTA** homologues (synthetic procedures are based on Ref. [10]), the achiral N,N',N''-tris(dodecyl)benzene-1,3,5-trithioamide **thioBTA-C12** and the chiral left-handed (*3S*)-N,N',N''-tris(3,7-dimethyloctyl)benzene-1,3,5-trithioamide **thioBTA-C8-S**, see Fig. 1a for the molecular structures. Amide-based analogues N,N',N''-tris(dodecyl)benzene-1,3,5-trisamide **BTA-C12** and (*3S*)-N,N',N''-tris(3,7-dimethyloctyl)benzene-1,3,5-trisamide **BTA-C8-S** were synthesized based on the procedure published earlier[16] and characterized for comparison.

Phase diagram and molecular packing

Based on differential scanning calorimetry (DSC), the melting point of **thioBTA-C12** and **thioBTA-C8-S** is found to be 254°C and 260°C, respectively, see SI Fig. S2 in the Supplementary Information (SI) section 1. The liquid-crystalline to crystalline (LC-to-Cr) phase transition occurs at around −5°C and 95°C for **thioBTA-C12** and **thioBTA-C8-S**, respectively[10]. In total, the ferroelectricity-friendly liquid-crystalline state is extended by ~80°C for **thioBTA-C12** and ~50°C for **thioBTA-C8-S**, as compared to their amide-based analogues[29], see Fig. 1b. It is worth noting that even in the crystalline state ($T < 95$°C) **thioBTA-**

C8-S demonstrates ferroelectric switching, similarly to **BTA-C6** and all the branched **BTA** homologues[3,7], while interesting and previously unobserved ferrielectric polarization switching behavior is found in the liquid-crystalline state, vide infra.

Regarding the molecular packing characteristics, little difference is found between thioamide- and amide-based materials. All four materials enter the columnar hexagonal liquid-crystalline state below the isotropic temperature with similar molecular packing parameters: an interdisc distance of 3.4 Å and an intercolumnar distance of 19.9 Å for **(thio)BTA-C8-S** at 150°C and 21 Å for **(thio)BTA-C12** at 36°C, as obtained from the small-angle X-ray scattering (SAXS) diffractograms[10,12].

Ferroelectric switching

Ferroelectric characterization was performed on spin-coated out-of-plane metal/ferroelectric/metal crossbar geometry devices with thermally evaporated aluminum as electrode material. All four materials demonstrated good film-forming properties in submicron-thick films with prominent self-assemblies as observed by AFM, see Fig. S3. For more details on device fabrication, characterization, and measurement geometry, we refer to the SI section 1. For what follows, it is important that the supramolecular polymers, i.e. the BTA stacks, that lie in-plane after deposition, are turned to stand out-of-plane by a field annealing procedure prior to further measurements, such that field and (axial) polarization are parallel.

Like the **BTA**-based analogues (see Fig. S4), **thioBTA-C12** and **thioBTA-C8-S** demonstrate stable ferroelectric switching with saturating ferroelectric hysteresis loops, as displayed in Fig. 1c-d. An improved saturated remnant polarization is observed in **thioBTA-C12** devices reaching $P_r \approx 35$ mC/m^2, as compared to ~30 mC/m^2 obtained for **BTA-C12**. This is close to the predicted geometrically available dipole density for an ideal lattice $P_r \approx 38$ mC/m^2. A remnant polarization of $P_r \approx 45$ mC/m^2, matching the theoretical estimations, was attained on **thioBTA-C8-S** devices, being nearly 30% higher than the 35 mC/m^2 of **BTA-C8-S**[29]. The experimentally observed increase in the remnant polarization can be explained by the higher dipole moment of thioamides μ = 5.1 D versus μ = 3.5-4.0 D characteristic to amide-based systems, as the macroscopic molecular packing parameters are closely matching. Note that at 70°C (Fig. 1c-d), the compared thio and regular BTA compounds (**thioBTA-C8-S** vs **BTA-C8-S** and **thioBTA-C12** vs **BTA-C12**) are in the same phase (crystalline and liquid-crystalline, respectively, see Fig. 1b). Hence, an alternative explanation for the differences in P_r due to compounds being in different phases can be ruled out.

An interesting but potentially misleading effect was observed when noble metal electrodes (e.g. Au, Pt) were used for contacts with **thioBTA** layers. At elevated temperatures (>100°C) in a slow voltage sweeping regime ($f \ll 1$ Hz), an extensive amount of charge was found when integrating the polarization switching current transients, reaching apparent charge densities of more than 1000 mC/m^2, see Fig. S5. Such large numbers cannot be explained by either molecular dipoles in the BTA, nor by induced dipoles on the metal surface.[30] Therefore, we tentatively attribute this effect to electrochemical reactions induced by sulphur in presence of noble metals[31]. Electrochemical reactions causing generation of high charge densities have been previously reported in pyrrole-substituted discotics[32]. When no noble metals are used for the contacts, **thioBTAs** act as regular ferroelectrics with polarization densities limited by the geometric density of switchable dipoles.

The temperature dependence of the coercive field E_c shows the activated behavior that is typical for BTAs, see Fig. S6. The data show higher and stronger temperature dependent coercive fields for the chiral materials, which is easily explained in terms of a higher structural order and a concomitantly lower density of (chiral) defects.[8,33] The data also show a lower and weaker temperature dependent coercive field for **thioBTA**-based materials than for the corresponding **BTA** materials. For comparison, E_c at 80°C and 25 Hz is ~22 V μm^{-1} for **thioBTA-C12** versus ~35 V μm^{-1} for **BTA-C12** and ~70 V μm^{-1} for **thioBTA-C8-S** versus ~210 V μm^{-1} for **BTA-C8-S**. The observed differences in absolute value and temperature dependence of the coercive field in solid state are somewhat surprising in view of previously reported differences in stability and cooperativity factor of the supramolecular homopolymers. De Windt et al. found the interactions of the **thioBTA** monomers to be more stable but less cooperative than those of **BTA**[11,34]. We tentatively attribute the difference to the fact that de Windt et al. studied supramolecular polymers in solution while we work in solid state where steric and Coulombic inter-columnar interactions are much more important.

The trend in depolarization activation energy barrier is in agreement with that of the coercive field, with lower activation energies for **thioBTA**. We find ~2.7 eV for **BTA-C8-S** vs. ~2.6 eV for **thioBTA-C8-S** and ~1.1 eV for **BTA-C12** vs. ~0.95 eV for **thioBTA-C12**, see Fig. 2c and S7c. These numbers also show a clear distinction between chiral and achiral homologues, the latter having an almost three times lower depolarization activation barrier. As discussed extensively in previous publications[8,29], the substantial polarization stabilization effect in enantiopure materials is related to low-disorder assemblies, namely, the absence of chiral defects and the ability to form large supramolecular structures via a cooperative supramolecular

polarization processes. As such, an (extrapolated) polarization retention of 10 years is reached already at 70°C for amide- and at 60°C for thioamide-based BTA-C8-S. In stark contrast, the polarization retention of linear **C12** homologues is 5-7 orders of magnitude lower under similar conditions. In the context of the previously characterized amide-based ferroelectrics, **thioBTA-C8-S** sits among the top-performing homologues retention-wise, see Fig. S7d.

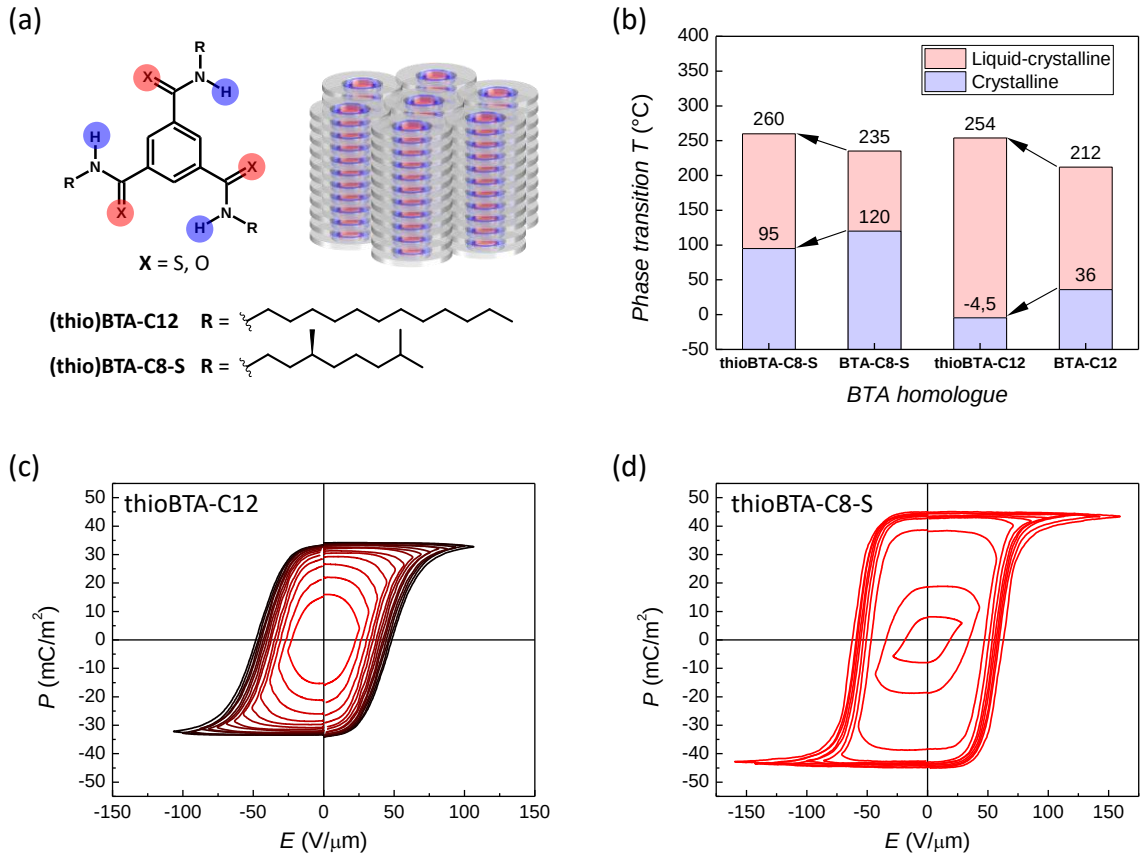

Figure 1. (a) Molecular structure and columnar hexagonal self-assembly of the studied molecules. (b) Phase diagram of **thioBTAs** and their analogous **BTAs** indicating extended liquid-crystalline phase. (c) Saturating polarization hysteresis with inner loops of **thioBTA-C12** and (d) **thioBTA-C8-S** obtained at 70°C, 25 Hz. The growing loops are obtained by increasing the maximum applied field from below (for the inner loops) to above (for the outer loops) the coercive field.

Ferrielectric switching

Apart from the differences discussed above, we found ferrielectric switching in **thioBTA-C8-S** devices at elevated temperatures. As shown in Fig. 2a, with increasing temperature the polarization switching current transient (*i.e.* the derivative of the hysteresis loop that is typically

of Gaussian form for conventional ferroelectrics) begins to split into two peaks when a temperature of around 90-95°C is reached, which is around the temperature the material enters its liquid-crystalline phase, *cf.* Fig. 1b. The peak positions of these current transients, which correspond to apparent coercive field values, are plotted versus the measurement temperature in panel (b). Dual features are also observed in the depolarization kinetics above 90-95°C, as seen in Fig. 2c. The fact that the full polarization, that corresponds to a 3:0-state, first decays into a state with reduced (~30-40% of the initial) polarization before, at longer times, completely vanishing, is a direct demonstration of the fact that the latter 2:1-state, that shows only one third of the original polarization, is the more stable one. The material is ferrielectric. Below this temperature – that is, in the crystalline state – no oddities manifest and the material acts as a regular ferroelectric. Characteristics of the neither the linear homologue **thioBTA-C12** nor the amide-based **BTA-C8-S** do reveal any feature splitting at elevated temperatures, see also Fig. S8a.

ThioBTA-C8-S demonstrates a clear and stable ferrielectric state in the liquid-crystalline phase. The total polarization is independent of temperature whilst the two peaks share the portion of the total polarization with a ratio of 2:1, see Fig. S8b. This ratio clearly corresponds to the previously mentioned switching mechanism via 1:2 conformers (↑↓↓ arrangement of helices within a column) predicted by the DFT/MD simulations. Note that the fact that the first switching peak has twice the area of the second peak implies that the switching sequence is 3:0→1:2→0:3. In contrast to the equilibration process studied in Fig. 2c, the kinetic experiment of polarization reversal thus shows (↑↑↑) changing to (↑↓↓) and straight to (↓↓↓) without an intermediate state; that is, no indications of a three-step kinetic 3:0→2:1→1:2→0:3 pathway have been observed. Interestingly, while having a similar **thioBTA** core, the dodecyl tailed molecule **thioBTA-C12** does not show ferrielectric switching at elevated temperatures. As discussed above, linear-tailed achiral mixtures are likely to form shorter and more disordered supramolecular aggregates, as compared to the enantiopure chiral-tailed analogues, suggesting that long-range order is a necessary but not sufficient condition to observe ferrielectric behavior
in BTA[11].

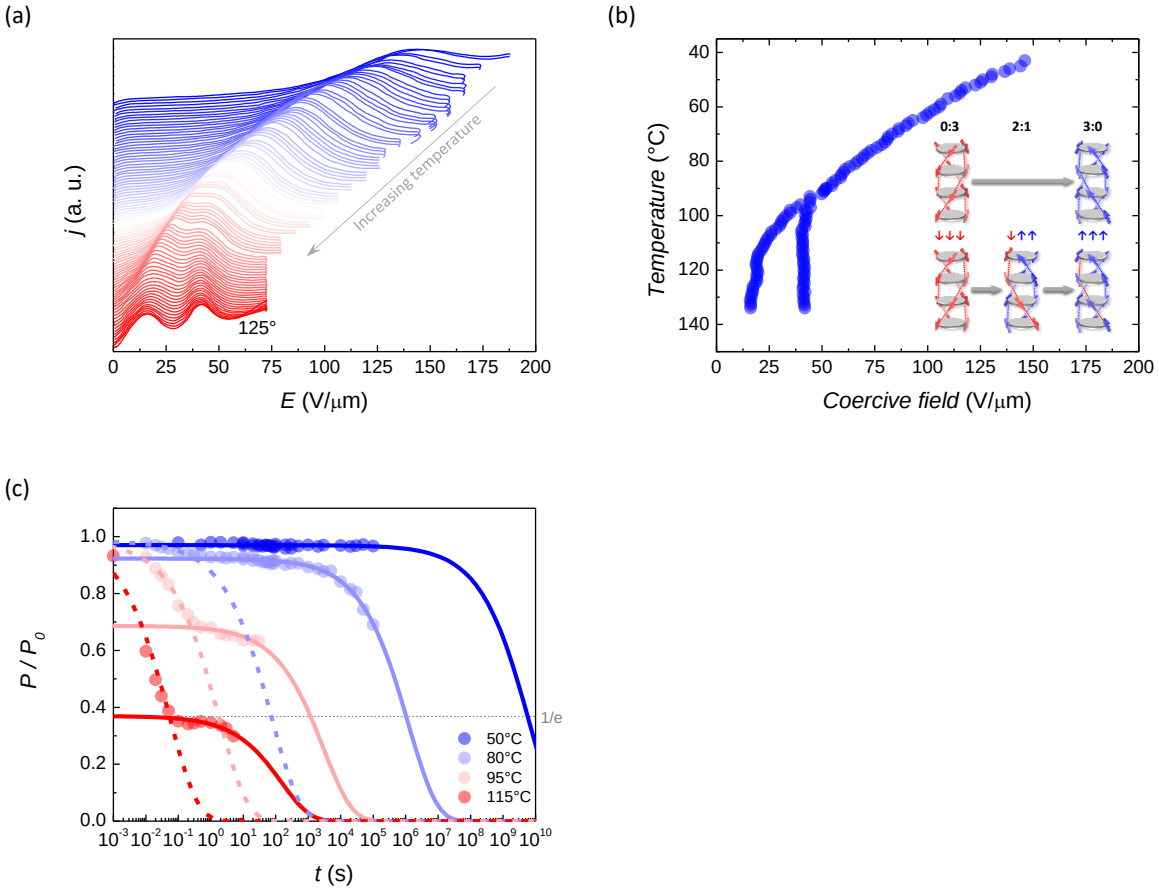

Figure 2. (a) Emergence of double features in the polarization switching current of **thioBTA-C8-S** at temperatures above 90-95°C. The *j*-*E* curves are displayed with an offset along the *y*-axis. Corresponding apparent coercive field values are given in panel (b). The inset illustrates the proposed mechanism of macrodipole switching via intermediate 2:1 conformers, in contrast to the single-step 0:3 to 3:0 switching scenario that is typical to **BTAs**. (c) Thermal depolarization kinetics showing two depolarization regimes, attributable to polarization relaxation via intermediate states (lines are fits to a stretched exponential function $\sim\exp[-(t/\tau)^{\beta}]$ with $\beta = 0.5$, dashed and solid lines indicating first (3:0→1:2) and second (1:2→0:3) depolarization rate, respectively). Full depolarization is considered as full randomization of macrodipoles – zero net macroscopic polarization.

Although we are not aware of specific theoretical calculations of thioamide-based materials, some further insight in the origins of the ferrielectric switching can be obtained from previously reported DFT/MD simulations on molecular stacks of amide-based molecules. Previously, Balasubramanian et al. used DFT/MD computations on amide-based molecules to predict that individual helices in trisamides can be of different polarity[9,18,19]. In fact, the asymmetric 2:1

helix configuration (↑↑↓) was found to be energetically favorable over the unidirectional case (↑↑↑). Most importantly, an increased stabilization effect of 2:1 and 1:2 conformations was obtained with larger oligomer size[9]. This could be an explanation why no ferrielectric features are observed in the (relatively) disordered linear-tailed **thioBTA-C12**, as compared to the chiral-tailed enantiopure **thioBTA-C8-S**. On basis of DFT/MD as well as kinetic Monte Carlo simulations, Cornelissen et al. argued that in **BTAs** the 2:1 state, being the preferred initial no-field state, becomes irrelevant once an external electric field is applied, after which the 3:0→0:3 pathway is the dominant one[8]. This is contradicted by the current experimental findings that show that in well-ordered **thioBTA** molecular stacks, the 3:0→1:2→0:3 mechanism is more likely when the system is in the liquid crystalline phase; in the crystalline phase, the 3:0→0:3 pathway is still dominant, possibly because the larger fields that are needed to induce switching make the intermediate 1:2 states kinetically inaccessible.

Piezoelectric response

Based on the previous knowledge of the piezoelectric properties of amide-based **BTA** homologues[4], we measured the converse piezoelectric response of **thioBTA-C8-S** Al/Al capacitor devices using a double-beam laser interferometer (DBLI). For experimental details see SI Section 1. Like the previously studied **BTA**-based systems, the experimentally observed negative piezoelectricity of **thioBTA-C8-S**, see Fig. 3, is not in line with the positive nanoscopic mechanism predicted by the DFT/MD simulations: in Ref. [4] we have shown that the energy dependence on the dihedral angle translates into a positive nanoscopic d_{33}. We thus suggest that the same morphology-related dimensional effect that governs the negative macroscopic large- and small-signal piezoelectric response of **BTAs**, also does so for **thioBTA**[4]. In this model, the (softer) disordered regions between (stiffer) molecular stacks are preferentially compressed by external stress, leading to a higher dipole density upon compression and, therefore, a negative d_{33}.[35]

In the ferroelectric state below 90-95°C, the behavior of **thioBTA-C8-S** is very similar to that previously observed in amide-based short-tailed **BTA-C6** devices[4], see Fig. 3a. The large-signal strain-field butterfly loops of **thioBTA-C8-S** have a strongly expressed linear dependence with a negative slope after polarization reversal that is characterized by the large-signal piezoelectric constant $d_{33,LS}$ reaching −5 pm/V, showing a weakly increasing trend with cooling, see Fig. S9. To compare, $d_{33,LS}$ up to −20 pm/V was found in short-tailed linear **BTA-C6** with a remnant polarization of P_r 60 mC/m^2 and −8 pm/V in **BTA-C8** with P_r 45 mC/m^2.

Considering the similar remnant polarization value of **thioBTA-C8-S**, the slightly reduced $d_{33,LS}$ can be related to either a higher mechanical stiffness as this chiral-tailed material is in its crystalline state below 90-95°C, or the reduced disorder discussed above.

A steep strain overshoot is observed as upward pointing 'ears' in Fig. 3a, which matches the polarization switching current peak, see Fig. S10a black solid line. The effect remains present, irrespective of temperature or probing frequency, see Fig. S11a-d. We previously noticed this phenomenon in **BTAs** and explained it as a transient variation of material stiffness, or Young's modulus, upon polarization switching, leading to a minimum in stiffness when the orientation of macrodipoles is randomized, that is, around the coercive field. [4] To reverse polarization, the H-bonded network of microdipoles must be broken and reestablished within the molecular stacks, causing a change in mechanical properties of the entire macroscopic layer. We emphasize that this is a transient effect and after full polarization reversal, a purely linear piezostrictive behavior is observed with the strain being linearly proportional to the electric field $S_{33} = d_{33}E$. Also, the piezoelectric constant is related to other (electro)mechanical material properties via $d_{33} = 2Q_{33}\varepsilon\varepsilon_0 P_r$, where the electrostriction coefficient $Q_{33} = \gamma_{33}/Y_{33}$ and thus d_{33} is inversely proportional to the Young's modulus Y_{33}. Very good fits of the strain-field loops can be produced by including a Gaussian variation of the mechanical stiffness into the linear strain field dependence, see Fig. S11e.

In the ferrielectric state above 90-95°C, the piezoelectric effect remains negative. However, double features are revealed in the strain-field loops that correspond to the two-step polarization switching explained earlier in the text. At lower frequencies, no reliable static longitudinal large-signal d_{33} constant can be extracted in this case due to depolarization-related artefacts, yet at 100 Hz probe frequency and 100°C, $d_{33} = -5.7$ pm/V can be extracted, see Fig. 3a, red line. Yet, owing to the mechanical softening effect, the dynamic transient longitudinal piezoelectric constant, obtained as the derivative of strain-field characteristics, can exceed ±400 pm/V, see Fig. S11f.

Small-signal longitudinal piezoelectric response and small-signal capacitance were measured using DBLI by applying a staircase-like voltage signal with a superimposed high-frequency sinusoidal voltage signal. Archetypal negative piezoelectric $d_{33,ss}$ loops were obtained in the ferroelectric phase, that is at temperatures below 90-95°C, see Fig. 3b. Similar to the large-signal case, a transition to an anomalous double-featured form occurs when entering the ferrielectric state. The shape of $d_{33,ss}$ reflects the characteristic stepped shape of P_r due to the linear proportionality of d_{33} and P_r. As for the previously studied **BTA** homologues, the zero-

field $d_{33,ss}$ is found to be smaller than under large-signal conditions and ranges from −1.9 pm/V at 70°C to −5.1 pm/V at 100°C, see Fig. S9.

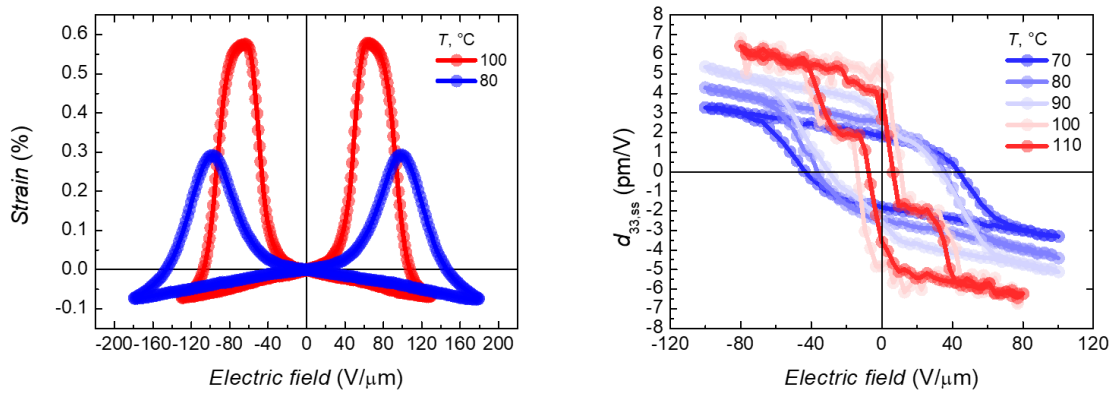

Figure 3. Converse piezoelectric response of **thioBTA-C8-S** capacitor devices at different temperature (a) under large-signal conditions and (b) under small-signal conditions.

Conclusions

We have investigated the effect of thioamide substitution in an archetypal C3-symmetry discotic molecule with linear achiral dodecyl (**thioBTA-C12**) and branched chiral left-handed 3,7-dimethyloctyl (**thioBTA-C8-S**) peripheral tails. Thioamide-based materials were compared with their amide-based counterparts in terms of molecular packing properties, thermotropic behavior and phase transitions, as well as in terms of ferroelectric and piezoelectric characteristics in thin-film spin-coated crossbar Al/**(thio)BTA**/Al capacitor devices.

ThioBTAs demonstrated textbook-like ferroelectric switching (similarly to **BTAs**) with up to 30% higher remnant polarization due to the higher microdipole moment of thioamides (~5 D vs. ~3.5 D), as the molecular packing parameters are matching for corresponding **thioBTA** and **BTA** molecules. In contrast, the coercive field and polarization retention were found to be lower and with a weaker temperature dependence (that is, lower activation energy).

The liquid-crystalline phase was found to be extended for **thioBTAs** both due to a higher melting point (or clearing, Curie temperature) and lower Cr-to-LC transition temperature. Interestingly, temperature-dependent polarization switching measurements revealed that in its liquid-crystalline state, the chiral **thioBTA-C8-S** demonstrates previously theoretically predicted (by DFT/MD simulations of amide-based systems) but never experimentally observed macrodipole switching mechanism via intermediate states. For the first time, a

pronounced helix-by-helix polarization reversal, manifesting itself as asymmetric double-features in *j-E*, *P-E*, *S-E* and depolarization characteristics, was observed, indicating ferrielectric switching. Ferrielectric switching is only found in chiral-tailed **thioBTA-C8-S** and not the **thioBTA-C12**, which we attribute to the stabilization effects related to longer, less disordered self-assemblies of the former.

Further, we found anomalous – negative – piezoelectricity in the ferroelectric as well as the ferrielectric phase of **thioBTA-C8-S**. The measured converse longitudinal piezoelectric constant reached d_{33} = −5-6 pm/V both under small- and large-signal conditions. This value is slightly lower than d_{33} = −8 pm/V previously found in **BTA-C8** with a matching remnant polarization ~45 mC/m^2. Similar to the **BTA** case, the proposed underlying mechanism of the negative piezoelectricity is the macroscopic dimensional effect. In line with previous work, we therefore explain this difference in d_{33} by reduced layer disorder and higher mechanical stiffness, both related to the chiral purity of the **thioBTA-C8-S**. In general, negative piezoelectricity is an exotic phenomenon limited to few materials systems, including the ferroelectric polymer **P(VDF:TrFE)**, short-tailed **BTA** and now also **thioBTA-C8-S**.

Based on the presented results, **thioBTAs**, and **thioBTA-C8-S** in particular, are an intriguing molecular system, carrying unique properties, including ferrielectricity and negative piezoelectricity, that arise from the high dipole moment (from thioamide) and the tail-governed chiral purity leading to highly cooperative supramolecular self-assembly and unusual collective polarization switching processes.

Acknowledgements

We would like to thank Prof. Beatriz Noheda Pinuaga for the opportunity to use the piezoelectric response measurement equipment and Anja R. A. Palmans and Tim D. Cornelissen for stimulating discussions and commenting on the manuscript. We also acknowledge technical support and help from Jacob Baas and Yingfen Wei during the piezoelectric measurements. I.U. acknowledges funding by Vetenskapsrådet (project nr. 2015-03813). M.G.I. thanks Santander Talent Attraction Research (STAR2) and financial support from Spanish MINECO (PID2021-125429NA-I00). M.K. thanks the Carl Zeiss Foundation for financial support.

References

(1) Nguyen, M. L.; Cho, B. K. Ferroelectrically Switchable Axial Polarization in Columnar Liquid Crystalline Phases. *Chemistry – A European Journal* **2020**, *26* (31), 6964–6975. https://doi.org/10.1002/CHEM.201904884.

(2) Stals, P. J. M.; Everts, J. C.; de Bruijn, R.; Filot, I. A. W.; Smulders, M. M. J.; Martín-Rapún, R.; Pidko, E. A.; de Greef, T. F. A.; Palmans, A. R. A.; Meijer, E. W. Dynamic Supramolecular Polymers Based on Benzene-1,3,5-Tricarboxamides: The Influence of Amide Connectivity on Aggregate Stability and Amplification of Chirality. *Chemistry - A European Journal* **2010**, *16* (3), 810–821. https://doi.org/10.1002/chem.200902635.

(3) Urbanaviciute, I.; Meng, X.; Cornelissen, T. D.; Gorbunov, A. V.; Bhattacharjee, S.; Sijbesma, R. P.; Kemerink, M. Tuning the Ferroelectric Properties of Trialkylbenzene-1,3,5-Tricarboxamide (BTA). *Advanced Electronic Materials* **2017**, *3* (7), 1600530. https://doi.org/10.1002/aelm.201600530.

(4) Urbanaviciute, I.; Meng, X.; Biler, M.; Wei, Y.; Cornelissen, T. D.; Bhattacharjee, S.; Linares, M.; Kemerink, M. Negative Piezoelectric Effect in an Organic Supramolecular Ferroelectric. *Materials Horizons* **2019**, *6* (8), 1688–1698. https://doi.org/10.1039/C9MH00094A.

(5) Casellas, N. M.; Urbanaviciute, I.; Cornelissen, T. D.; Berrocal, J. A.; Torres, T.; Kemerink, M.; García-Iglesias, M. Resistive Switching in an Organic Supramolecular Semiconducting Ferroelectric. *Chemical Communications* **2019**, *55* (60), 8828–8831. https://doi.org/10.1039/C9CC02466B.

(6) Gorbunov, A. V.; Garcia Iglesias, M.; Guilleme, J.; Cornelissen, T. D.; Roelofs, W. S. C. C.; Torres, T.; González-Rodríguez, D.; Meijer, E. W.; Kemerink, M.; Iglesias, M. G.; Guilleme, J.; Cornelissen, T. D.; Roelofs, W. S. C. C.; Torres, T.; González-Rodríguez, D.; Meijer, E. W.; Kemerink, M. Ferroelectric Self-Assembled Molecular Materials Showing Both Rectifying and Switchable Conductivity. *Science Advances* **2017**, *3* (9), e1701017. https://doi.org/10.1126/sciadv.1701017.

(7) Urbanaviciute, I.; Bhattacharjee, S.; Biler, M.; Lugger, J. A. M.; Cornelissen, T. D.; Norman, P.; Linares, M.; Sijbesma, R. P.; Kemerink, M. Suppressing Depolarization by Tail Substitution in an Organic Supramolecular Ferroelectric. *Physical Chemistry Chemical Physics* **2019**, *21* (4), 2069–2079. https://doi.org/10.1039/C8CP06315J.

(8) Cornelissen, T. D.; Biler, M.; Urbanaviciute, I.; Norman, P.; Linares, M.; Kemerink, M. Kinetic Monte Carlo Simulations of Organic Ferroelectrics. *Physical Chemistry Chemical Physics* **2019**, *21* (3), 1375–1383. https://doi.org/10.1039/C8CP06716C.

(9) Bejagam, K. K.; Fiorin, G.; Klein, M. L.; Balasubramanian, S. Supramolecular Polymerization of Benzene-1,3,5-Tricarboxamide: A Molecular Dynamics Simulation Study. *The Journal of Physical Chemistry B* **2014**, *118* (19), 5218–5228. https://doi.org/10.1021/jp502779z.

(10) Mes, T.; Cantekin, S.; Balkenende, D. W. R.; Frissen, M. M. M.; Gillissen, M. A. J.; De Waal, B. F. M.; Voets, I. K.; Meijer, E. W.; Palmans, A. R. A. Thioamides: Versatile Bonds To Induce Directional and Cooperative Hydrogen Bonding in Supramolecular Polymers. *Chemistry - A European Journal* **2013**, *19* (26), 8642–8649. https://doi.org/10.1002/chem.201204273.

(11) Kulkarni, C.; Meijer, E. W.; Palmans, A. R. A. Cooperativity Scale: A Structure–Mechanism Correlation in the Self-Assembly of Benzene-1,3,5-Tricarboxamides. *Accounts of Chemical Research* **2017**, *50* (8), 1928–1936. https://doi.org/10.1021/acs.accounts.7b00176.

(12) Stals, P. J. M.; Smulders, M. M. J.; Martín-Rapún, R.; Palmans, A. R. A.; Meijer, E. W. Asymmetrically Substituted Benzene-1,3,5-Tricarboxamides: Self-Assembly and Odd-

Even Effects in the Solid State and in Dilute Solution. *Chemistry - A European Journal* **2009**, *15* (9), 2071–2080. https://doi.org/10.1002/chem.200802196.
(13) Palmans, A. R. A.; Meijer, E. W. Amplification of Chirality in Dynamic Supramolecular Aggregates. *Angewandte Chemie - International Edition* **2007**, *46* (47), 8948–8968. https://doi.org/10.1002/anie.200701285.
(14) Smulders, M. M. J.; Stals, P. J. M.; Mes, T.; Paffen, T. F. E.; Schenning, A. P. H. J.; Palmans, A. R. A.; Meijer, E. W. Probing the Limits of the Majority-Rules Principle in a Dynamic Supramolecular Polymer. *Journal of the American Chemical Society* **2010**, *132* (2), 620–626. https://doi.org/10.1021/ja9080875.
(15) Markvoort, A. J.; Ten Eikelder, H. M. M.; Hilbers, P. A. J.; De Greef, T. F. A.; Meijer, E. W. Theoretical Models of Nonlinear Effects in Two-Component Cooperative Supramolecular Copolymerizations. *Nature Communications* **2011**, *2* (1), 509. https://doi.org/10.1038/ncomms1517.
(16) Smulders, M. M. J.; Filot, I. A. W.; Leenders, J. M. A.; Van Der Schoot, P.; Palmans, A. R. A.; Schenning, A. P. H. J.; Meijer, E. W. Tuning the Extent of Chiral Amplification by Temperature in a Dynamic Supramolecular Polymer. *Journal of the American Chemical Society* **2010**, *132* (2), 611–619. https://doi.org/10.1021/ja908053d.
(17) Aparicio, F.; García, F.; Sánchez, L. Supramolecular Polymerization of C3-Symmetric Organogelators: Cooperativity, Solvent, and Gelation Relationship. *Chemistry - A European Journal* **2013**, *19* (9), 3239–3248. https://doi.org/10.1002/chem.201202584.
(18) Bejagam, K. K.; Kulkarni, C.; George, S. J.; Balasubramanian, S. External Electric Field Reverses Helical Handedness of a Supramolecular Columnar Stack. *Chemical Communications* **2015**, *51* (89), 16049–16052. https://doi.org/10.1039/C5CC05569E.
(19) Kulkarni, C.; Reddy, S. K.; George, S. J.; Balasubramanian, S. Cooperativity in the Stacking of Benzene-1,3,5-Tricarboxamide: The Role of Dispersion. *Chemical Physics Letters* **2011**, *515* (4–6), 226–230. https://doi.org/10.1016/j.cplett.2011.09.028.
(20) Bejagam, K. K.; Balasubramanian, S. Supramolecular Polymerization: A Coarse Grained Molecular Dynamics Study. *The Journal of Physical Chemistry B* **2015**, *119* (17), 5738–5746. https://doi.org/10.1021/acs.jpcb.5b01655.
(21) Zehe, C. S.; Hill, J. A.; Funnell, N. P.; Kreger, K.; van der Zwan, K. P.; Goodwin, A. L.; Schmidt, H.-W.; Senker, J. Mesoscale Polarization by Geometric Frustration in Columnar Supramolecular Crystals. *Angewandte Chemie International Edition* **2017**, *56* (16), 4432–4437. https://doi.org/10.1002/anie.201612122.
(22) Scott, J. F.; Morrison, F. D.; Slawin, A. M. Z.; Lightfoot, P.; Clulow, R.; Gherson, A. S. A.; Bumstead, A. M.; Gardner, J.; Capelli, S. C.; Probert, M. R.; Sahoo, S.; Young, J. S.; Katiyar, R. S.; Salje, E. K. H. Ferrielectricity in the Metal-Organic Ferroelectric Tris-Sarcosine Calcium Chloride. *Physical Review B* **2017**, *95* (9), 094119. https://doi.org/10.1103/PHYSREVB.95.094119/FIGURES/10/MEDIUM.
(23) Fu, Z.; Chen, X.; Li, Z.; Hu, T.; Zhang, L.; Lu, P.; Zhang, S.; Wang, G.; Dong, X.; Xu, F. Unveiling the Ferrielectric Nature of PbZrO3-Based Antiferroelectric Materials. *Nature Communications 2020 11:1* **2020**, *11* (1), 1–8. https://doi.org/10.1038/s41467-020-17664-w.
(24) Glogarová, M.; Sverenyák, H.; Fukuda, A.; Takezoe, H. Electrooptic Properties of Chiral Smectic Liquid Crystals with a Dipolar Order. *http://dx.doi.org/10.1080/02678299308027661* **2006**, *14* (2), 463–468. https://doi.org/10.1080/02678299308027661.
(25) Jaradat, S.; Brimicombe, P. D.; Roberts, N. W.; Southern, C.; Gleeson, H. F. Asymmetric Switching in a Ferrielectric Liquid Crystal Device. *Applied Physics Letters* **2008**, *93* (15), 153506. https://doi.org/10.1063/1.3001933.

(26) Takezoe, H.; Lee, J.; Ouchi, Y.; Fukuda, A. Ferrielectric Chiral Smectic Liquid Crystalline Phase. *http://dx.doi.org/10.1080/00268949108035660* **2006**, *202* (1), 85–90. https://doi.org/10.1080/00268949108035660.
(27) Emelyanenko, A. V.; Pozhidaev, E. P.; Molkin, V. E.; Shtykov, N. M. Antiferroelectric and Ferrielectric Liquid-Crystal Display: Electrically Controlled Birefringence Color Switch as a New Mode. *Journal of the Society for Information Display* **2008**, *16* (8), 811–818. https://doi.org/10.1889/1.2966442.
(28) Kumar, J.; Prasad, V. Ferroelectric Nematic and Ferrielectric Smectic Mesophases in an Achiral Bent-Core Azo Compound. *The Journal of Physical Chemistry B* **2018**, *122* (11), 2998–3007. https://doi.org/10.1021/ACS.JPCB.7B11733.
(29) Urbanaviciute, I.; Biler, M.; Cornelissen, T. D.; Palmans, A.; Linares, M.; Kemerink, M. *Experimental Indications for Electrically Switchable Chirality in BTA*; 2022.
(30) Bauert, T.; Zoppi, L.; Koller, G.; Garcia, A.; Baldridge, K. K.; Ernst, K.-H. Large Induced Interface Dipole Moments without Charge Transfer: Buckybowls on Metal Surfaces. *J. Phys. Chem. Lett.* **2011**, *2* (21), 2805–2809. https://doi.org/10.1021/jz2012484.
(31) Salvarezza, R. C.; Carro, P. The Electrochemical Stability of Thiols on Gold Surfaces. *Journal of Electroanalytical Chemistry* **2018**, *819*, 234–239. https://doi.org/10.1016/J.JELECHEM.2017.10.046.
(32) Meng, X.; Gorbunov, A. V.; Christian Roelofs, W. S.; Meskers, S. C. J.; Janssen, R. A. J.; Kemerink, M.; Sijbesma, R. P. Ferroelectric Switching and Electrochemistry of Pyrrole Substituted Trialkylbenzene-1,3,5-Tricarboxamides. *Journal of Polymer Science Part B: Polymer Physics* **2017**, *55* (8), 673–683. https://doi.org/10.1002/polb.24318.
(33) Cornelissen, T. D.; Urbanaviciute, I.; Kemerink, M. Microscopic Model for Switching Kinetics in Organic Ferroelectrics Following the Merz Law. *Phys. Rev. B* **2020**, *101* (21), 214301. https://doi.org/10.1103/PhysRevB.101.214301.
(34) De Windt, L. N. J.; Kulkarni, C.; Ten Eikelder, H. M. M.; Markvoort, A. J.; Meijer, E. W.; Palmans, A. R. A. Detailed Approach to Investigate Thermodynamically Controlled Supramolecular Copolymerizations. *Macromolecules* **2019**, *52* (19), 7430–7438. https://doi.org/10.1021/ACS.MACROMOL.9B01502/SUPPL_FILE/MA9B01502_SI_002.ZIP.
(35) Katsouras, I.; Asadi, K.; Li, M.; Van Driel, T. B.; Kjær, K. S.; Zhao, D.; Lenz, T.; Gu, Y.; Blom, P. W. M. M.; Damjanovic, D.; Nielsen, M. M.; de Leeuw, D. M. The Negative Piezoelectric Effect of the Ferroelectric Polymer Poly(Vinylidene Fluoride). *Nature Materials* **2016**, *15* (1), 78–84. https://doi.org/10.1038/nmat4423.